Applied Catalysis B: Environmental 91 (2009) 73–82

Contents lists available at ScienceDirect

Applied Catalysis B: Environmental

journal homepage: www.elsevier.com/locate/apcatb

Morphology tuning of supported MoS_2 slabs for selectivity enhancement of fluid catalytic cracking gasoline hydrodesulfurization catalysts

Yu Fan [a,b], Gang Shi [b], Haiyan Liu [b], Xiaojun Bao [a,b,*]

[a] State Key Laboratory of Heavy Oil Processing, China University of Petroleum, Beijing 102249, PR China
[b] The Key Laboratory of Catalysis, China National Petroleum Corp. (CNPC), China University of Petroleum, Beijing 102249, PR China

ARTICLE INFO

Article history:
Received 2 January 2009
Received in revised form 26 April 2009
Accepted 12 May 2009
Available online 19 May 2009

Keywords:
Fluid catalytic cracking gasoline
Selective hydrodesulfurization
Co–Mo–Mg/Al_2O_3
MoS_2 morphology tuning
Dispersion and stacking of supported MoS_2 slabs

ABSTRACT

A series of Co–Mo–Mg/Al_2O_3, K–Co–Mo–Mg/Al_2O_3, and Co–Mo/silica catalysts were prepared and characterized by means of N_2 adsorption, temperature-programmed desorption of ammonia (NH_3-TPD), high-resolution transmission electron microscopy (HRTEM), and Fourier transformed infrared (FT-IR) spectra of adsorbed NO. The physicochemical properties of the catalysts were correlated with their hydrodesulfurization and olefin hydrogenation activities. The results showed that the dispersion and stacking of supported MoS_2 were more important in influencing the selectivity of FCC gasoline hydrodesulfurization than the catalyst pore diameter and acidity. The compromise between the dispersion and the stacking of supported MoS_2 slabs was crucial to form the sufficient and accessible Co–Mo–S phases for achieving optimal hydrodesulfurization selectivity. The present results form a fundamental basis for developing highly effective catalysts for the selective hydrodesulfurization of fluid catalytic cracking gasoline to meet the strict regulations for ultra-low sulfur gasoline.

1. Introduction

Air pollution in urban regions caused by exhaust emissions from gasoline-powered motor vehicles has become a serious issue in both developed and developing countries due to the high content of sulfur compounds in most gasoline. Sulfur compounds can degrade the effectiveness of automobile catalytic converters for controlling NO_x, CO, and hydrocarbon emissions by poisoning three-way catalysts. Thus, most of the countries over the world have tightened their regulations on gasoline compositions, especially on the content of sulfur compounds. More than 90% of sulfur in a typical refinery gasoline pool comes from fluid catalytic cracking (FCC) gasoline [1] and thus the sulfur reduction of this stream plays an important role in clean gasoline production. It has been widely recognized that hydrotreating FCC gasoline is one of the most important deep desulfurization techniques, but the concomitant olefin saturation gives rise to a serious loss in gasoline octane number [2,3]. Therefore, selective hydrodesulfurization (HDS) that can minimize the loss in gasoline octane number is highly desired to meet the stricter regulations on sulfur content [4]. Many efforts have been made to improve the HDS selectivity of conventional sulfide-based catalysts (e.g. CoMo/Al_2O_3) by modifying their composition or surface properties, such as deactivation of CoMo/Al_2O_3 by a coking pretreatment [5,6], incorporation of potassium or potassium and phosphorus into CoMo/Al_2O_3 [7,8], and use of binary supports (TiO_2–Al_2O_3 [9,10] and MgO–Al_2O_3 [11,12]). However, many conclusions for enhancing the HDS selectivity of catalysts derived from these researches are contradictory.

As to Co–Mo–S active phases, Miller et al. thought that HDS and olefin hydrogenation (OHY) reactions occur on the same type of active sites of supported Co–Mo–S phases [13]. Nevertheless, there are also many evidences in favor of different types of active sites for HDS and OHY. It is well-known that the HDS activity is enhanced by incorporating Co into Mo sulfide, whereas little effect is observed on OHY activity [14,15]. Hatanaka et al. [16] proposed that there are three types of active sites for HDS, n-olefin hydrogenation, and iso-olefin hydrogenation on sulfided CoMo/Al_2O_3 catalysts by investigating the inhibiting effect of H_2S, but they did not mention the structure of the active sites. Choi et al. [17] proposed that the interfacial sites between sulfide phase and hydroxyl groups of the alumina support were responsible for OHY and the sulfur vacancies on the edge sites of MoS_2 slabs were very important for HDS. Candia et al. [18] pointed out that, compared with the so-called Type I Co–Mo–S phase of high dispersion, Type II Co–Mo–S phase of high stacking had the better HDS/OHY selectivity. In addition, it has been pointed out that decreasing the acidity of CoMo/Al_2O_3 can reduce the OHY activity more than the

* Corresponding author. Tel.: +86 010 89734836; fax: +86 010 89734979.
E-mail address: baoxj@cup.edu.cn (X. Bao).

0926-3373/$ – see front matter © 2009 Elsevier B.V. All rights reserved.
doi:10.1016/j.apcatb.2009.05.008

Table 1
Nomenclature of the oxidic catalysts with different compositions.

Catalyst	CoO (wt.%)	MoO_3 (wt.%)	MgO (wt.%)	K_2O (wt.%)	Support A1 (wt.%)	Support A2 (wt.%)	Support silica (wt.%)
CA1	3.0	14.0	3.0	–	80	–	–
C56A1-24A2	3.0	14.0	3.0	–	56	24	–
C48A1-32A2	3.0	14.0	3.0	–	48	32	–
C40A1-40A2	3.0	14.0	3.0	–	40	40	–
C24A1-56A2	3.0	14.0	3.0	–	24	56	–
CA2	3.0	14.0	3.0	–	–	80	–
CA1-K1	3.0	14.0	3.0	1.0	79	–	–
CA1-K2	3.0	14.0	3.0	2.0	78	–	–
CS1	2.5	12.0	–	–	–	–	85.5 (Silica-1)
CS2	2.5	12.0	–	–	–	–	85.5 (Silica-2)
CS3	2.5	12.0	–	–	–	–	85.5 (Silica-3)

HDS activity and thus increase the HDS selectivity [19,20]. Recently, it has been reported that the incorporation of mesoporous MCM-41 into $CoMo/Al_2O_3$ can improve the latter's HDS selectivity, showing the effect of support pore structure [21].

At present, many researchers are interested in the question which factor, supported metal sulfides, catalyst acidity or catalyst pore structure, is the most important for enhancing the HDS selectivity of supported sulfide catalysts, but it still has not been answered to the best of our knowledge. The present investigation attempts to answer this question. Herein, a series of Co–Mo–Mg/Al_2O_3, K–Co–Mo–Mg/Al_2O_3, and Co–Mo/silica catalysts were prepared and their acidity, pore structure, and structure of active metal sites were correlated with the HDS selectivity. On the basis of the correlation results, the foremost factor influencing HDS selectivity was determined.

2. Experimental

2.1. Catalyst preparation

A series of alumina supports with different pore structure were obtained by mixing two kinds of alumina A1 and A2 (both were provided by Shandong Aluminum Plant, PR China) in different proportions. The alumina supports were prepared as follows. First, the pseudoboehmite precursors of A1 and A2 were ground to particles of 500–800 mesh. Then, the two precursors were homogeneously blended according to the required weight ratios of A1 to A2. Finally, the resulting mixtures were shaped by extrusion, dried at 120 °C for 5 h, and calcined at 520 °C for 4 h. By the incipient wetness impregnation of the above supports successively with aqueous solutions of $Mg(NO_3)_2$, $(NH_4)_6Mo_7O_{24}$, and $Co(NO_3)_2$ (Beijing Chemical Co., PR China) according to the required metal loadings, a series of oxidic Co–Mo–Mg/γ-Al_2O_3 catalysts were prepared and their nomenclature and composition are summarized in Table 1. These catalysts are denoted as C*X*A1-*Y*A2, in which *X* is the weight percentage of A1 and *Y* the weight percentage of A2. The catalyst made only from A1 (surface area: 292 m^2/g, pore volume: 0.30 mL/g) is denoted as CA1 and the one made only from A2 (surface area: 201 m^2/g, pore volume: 0.51 mL/g) is denoted as CA2.

After each impregnation step, the solids were dried at 120 °C for 5 h, and calcined at 500 °C for 4 h. Mg was incorporated into the above catalysts to decrease the acidity of the alumina support [4] and weaken the interaction between alumina and Mo or Co because of the preferential Mg–Al interaction [2].

To solely evaluate the effects of acidity on the HDS and OHY activities, Catalyst CA1 was impregnated with aqueous solutions of KNO_3 according to the different potassium loadings. The obtained solids were dried at 120 °C for 5 h, and calcined at 500 °C for 4 h. The nomenclature and composition of the catalysts containing potassium are summarized in Table 1.

To solely evaluate the effect of pore structure on the HDS and OHY activities, Silica-1 (Qingdao Ocean Chemical Plant, PR China, surface area: 600 m^2/g, pore volume: 0.65 mL/g), Silica-2 (Qingdao Ocean Chemical Plant, PR China, surface area: 560 m^2/g, pore volume: 0.70 mL/g), Silica-3 (Qingdao Ocean Chemical Plant, PR China, surface area: 510 m^2/g, pore volume: 0.80 mL/g) were impregnated successively with aqueous solutions of $(NH_4)_6Mo_7O_{24}$ and $Co(NO_3)_2$ according to the required metal loadings, respectively. The obtained solids were dried at 120 °C for 5 h, and calcined at 500 °C for 4 h. The nomenclature and composition of the silica-supported catalysts are also summarized in Table 1.

2.2. Catalyst characterization

The contents of Co, Mo, Mg, and K in terms of the corresponding oxides in the catalysts were determined on a ZSX-100e X-ray fluorescence (XRF) analyzer (Rigaku Co., Japan). The surface area and pore volume measurements of the samples were conducted on a volumetric adsorption apparatus (ASAP 2405N, Micromeritics Co., Atlanta, GA) at −195 °C using N_2 as adsorbate. The samples were evacuated at 300 °C for 4 h under a vacuum of 1.33×10^{-3} Pa prior to analysis.

The number and strength distributions of the acid sites of the catalysts were studied by means of temperature-programmed desorption of ammonia (NH_3-TPD). First, the samples, each 100 mg, were heated from room temperature to 600 °C at a rate of 10 °C/min and then cooled down to 100 °C in a pure He flow. Then, ammonia was adsorbed at 100 °C for 20 min, and subsequently the samples were purged by a flowing He stream at 100 °C for 1 h to remove excessive and physically adsorbed NH_3. Finally, the samples were heated from 100 to 600 °C at a rate of 10 °C/min in a pure He flow and the desorption patterns were recorded. Ammonia evolved was trapped in a standard solution of HCl, and the redundant HCl was titrated by a standard solution of NaOH with an online automatic pH titrator until the pH value of the solution reaches 5.0 (i.e. the pH value of the NH_4Cl solution from the reaction between NH_3 and HCl). So, the amount of desorbed ammonia can be calculated according to the concentrations and volumes of the HCl and NaOH standard solutions consumed.

The morphology of the active phases on sulfided catalysts was characterized by high-resolution transmission electron microscopy (HRTEM) conducted on a Tecnai F-20 microscope (Philips Co., Netherlands) with a point-to-point resolution of 2.4 Å and equipped with a Link-ISIS-300 energy-dispersive X-ray spectrometer (EDX). The solids to be measured were ultrasonically dispersed in cyclohexane and testing samples were prepared by dropping the dispersed suspensions on carbon-coated copper grids.

Table 2
Properties of the feeding FCC gasoline.

Density (20 °C) (g/cm^3)	S (μg/g)	RON	Group composition (v%)				
			n-Paraffin	i-Paraffin	Olefin	Naphthene	Aromatics
0.724	850	92.6	4.3	25.0	42.7	7.8	20.2

Table 3
Physicochemical properties and reaction performances of Catalysts CA1, C*X*A1-*Y*A2, and CA2.

Catalyst	Pore structure			Acidity	MoS_2 morphology		Activity	
	S_g [a] (m^2/g)	V_p [b] (mL/g)	D_p [c] (nm)	A_a [d] (μmol NH_3/g_{cat})	$\bar{L}$ [e] (nm)	$\bar{N}$ [e]	HDS (%)	OHY (%)
CA1	264	0.25	3.8	324	2.3	1.1	61	48
C56A1-24A2	244	0.28	4.6		3.6	1.7	68	37
C48A1-32A2	229	0.32	5.6	278	4.1	2.3	81	21
C40A1-40A2	215	0.35	6.5		4.7	2.6	74	19
C24A1-56A2	192	0.37	7.7		5.2	3.1	69	17
CA2	176	0.41	9.3	212	5.6	3.8	60	14

[a] BET surface area.
[b] Pore volume.
[c] Mean pore diameter ($4V_p/S_g$).
[d] Acid amount obtained by NH_3-TPD.
[e] Average slab length and stacking layer number obtained by the statistics analysis from different HRTEM micrographs.

Fourier transformed infrared (FT-IR) spectra of adsorbed NO over the sulfided catalysts were measured using a FT-IR spectrometer (Nicolet Co., Magna 560). The wafers of the catalyst samples were introduced into the FT-IR cell and in situ sulfided in a 10% H_2S/H_2 stream at 360 °C for 1 h. After sulfidation, the H_2S gas mixture and chemisorbed H_2S were removed by flushing the cell with purified He at 360 °C for 3 h. Then, the samples were slowly cooled down to ambient temperature in a purified He flow and evacuated to 10^{-4} Torr. After the background spectra were measured at a resolution of 4 cm^{-1}, the samples were exposed to a 10% NO/He stream for 0.5 h, followed by flushing with purified He for 1 h. Finally, the IR spectra of adsorbed NO were obtained by subtracting the background spectra.

2.3. Catalytic performance assessments

The catalytic performance assessments were carried out in a flow-type apparatus designed for continuous operation. This apparatus consists of a gas-feeding system controlled by a mass flowmeter and a syringe pump liquid-feeding system. The reactor, with an internal diameter of 10 mm, was loaded with a catalyst sample of ca. 4 g. The hydrocarbon compositions of the feedstock and products were determined using an Agilent 1790 gas chromatograph installed with a flame ionization detector (FID) and a HP-PONA capillary column (50 m × 0.2 mm). The research octane numbers (RONs) of the feedstock and products were obtained on the ASTM-CFR octane rating engine (Ethyl Chemical Co., America). The contents of total sulfur in the feedstock and products were measured by a WK-2C microcoulombmeter (Jiangsu Jiangfen Electroanalytical Instrument Co., PR China).

In all runs, the catalysts to be tested were brought to identical reaction conditions. First, the oxidic catalysts were presulfurized at 230, 260, and 290 °C for 3 h, by a stream containing 3 wt.% CS_2 in cyclohexane through the catalyst bed in the presence of pure H_2. Then, FCC gasoline was fed into the reactor at a predetermined flow rate after the temperature was decreased to the reaction temperature. Finally, the reaction was carried out at 240 °C, a total pressure of 1.4 MPa, a FCC gasoline liquid hourly space velocity (LHSV) of 4.0 h^{-1}, and a volumetric ratio of H_2 to oil of 500. After a stabilization period of 8 h, the reaction products were collected and analyzed.

The conversion of total sulfur and the conversion of olefin hydrogenation were calculated as follows:

$$\mathrm{HDS}\,(\%) = \frac{S_f - S_p}{S_f} \times 100 \tag{1}$$

$$\mathrm{OHY}\,(\%) = \frac{O_f - O_P}{O_f} \times 100 \tag{2}$$

where S_f and S_p are the mass fractions of total sulfur in the feedstock and products, respectively; O_f and O_p the volume fractions of olefins in the feedstock and products, respectively.

The selectivity factor (SF) is defined as the ratio of HDS activity to OHY activity and expressed by:

$$\mathrm{SF} = \frac{\ln(S_f/S_p)}{\ln(O_f/O_p)} \tag{3}$$

The RON loss is defined as:

$$\mathrm{RON\,loss} = \mathrm{RON}_f - \mathrm{RON}_p \tag{4}$$

where RON_f and RON_p are the RONs of the feedstock and products, respectively.

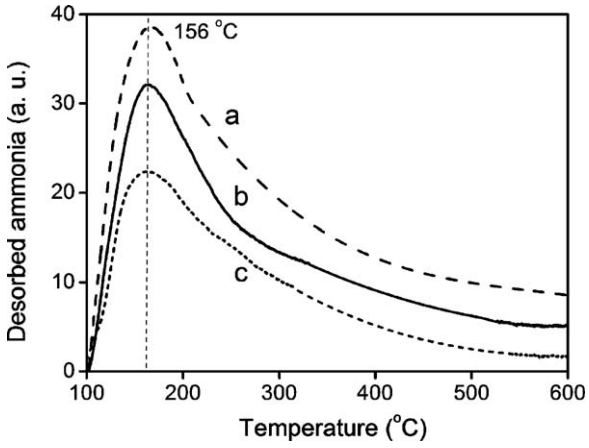

Fig. 1. NH_3-TPD profiles of the oxidic catalysts (a) CA1, (b) C48A1-32A2, and (c) CA2.

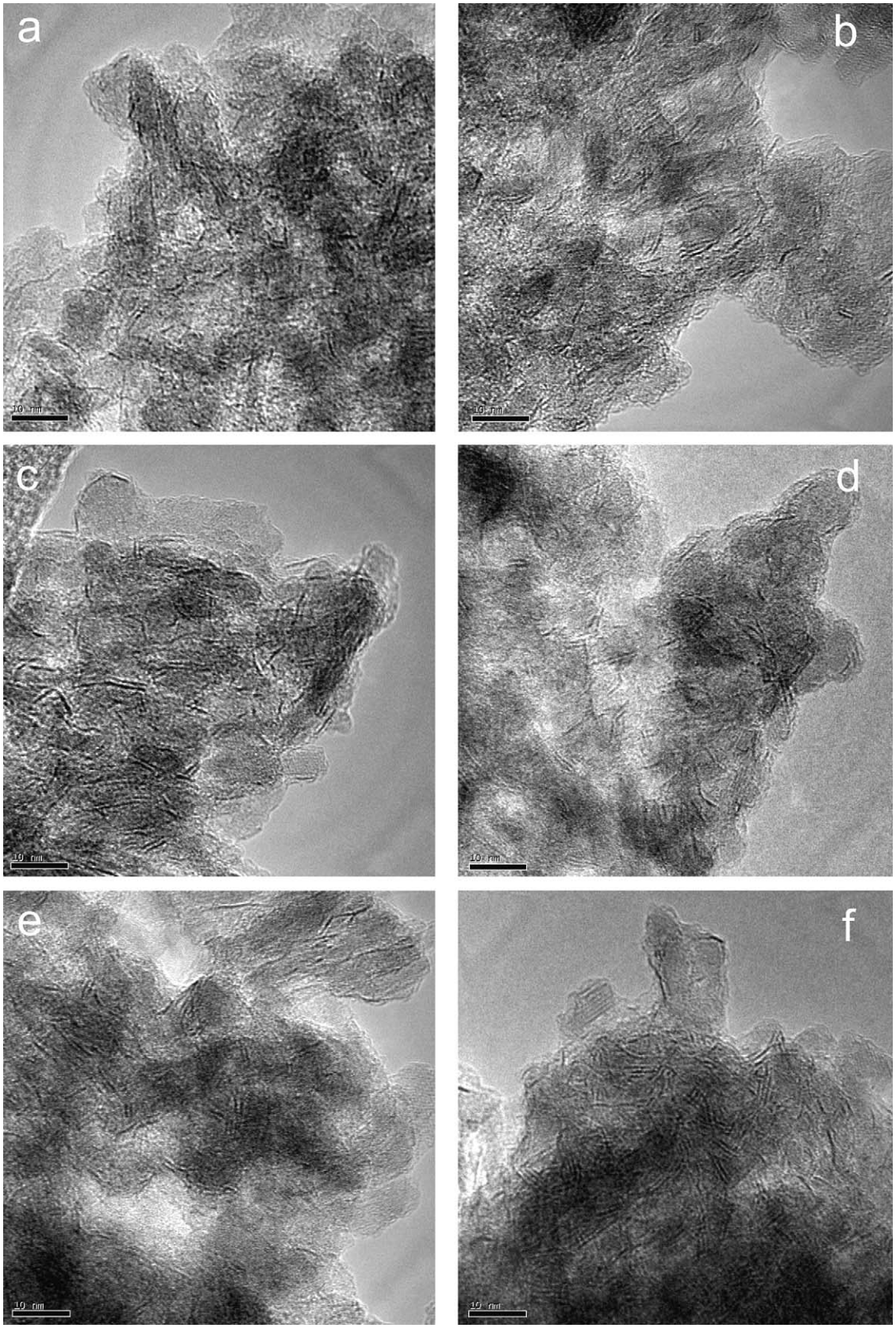

Fig. 2. HRTEM micrographs of the sulfided catalysts (a) CA1, (b) C56A1-24A2, (c) C48A1-32A2, (d) C40A1-40A2, (e) C24A1-56A2, and (f) CA2.

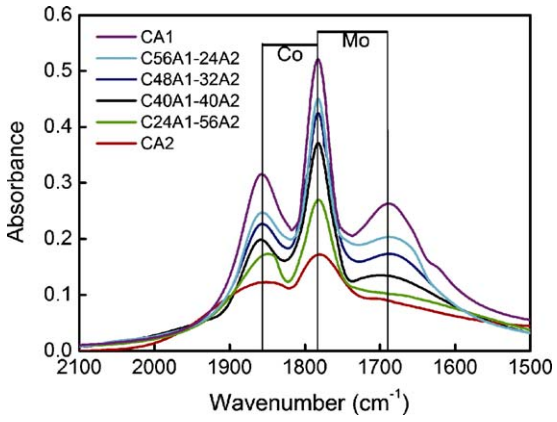

Fig. 3. IR spectra of adsorbed NO on sulfided Catalysts CA1, CXA1-*YA2*, and CA2.

The properties of the feeding FCC gasoline are listed in Table 2.

3. Results

3.1. N_2 adsorption

The pore structure properties of oxidic Catalysts CA1, CXA1-*YA2*, and CA2 measured by the N_2 adsorption method are presented in Table 3. The catalyst surface area decreases and the catalyst pore volume and mean pore diameter increase with the decreasing content of alumina A1 or the increasing content of alumina A2, in accordance with the texture properties of the two alumina supports.

3.2. NH_3-TPD

The acidity properties of oxidic Catalysts CA1, C48A1-32A2, and CA2 are shown in Fig. 1. The three catalysts have almost the same acid strength, as indicated by their very close maximum NH_3 desorption temperatures at about 156 °C that are widely considered as the index of acid strength [22]. The acid amounts of the catalysts calculated from the NH_3-TPD profiles decrease in the order CA1(324 μmol NH_3/g_{cat}) > C48A1-32A2(278 μmol NH_3/g_{cat}) > CA2(212 μmol NH_3/g_{cat}), indicating more accessible acid sites on the catalysts with larger surface area.

3.3. HRTEM

The catalytic performance of MoS_2-based HDS catalysts is related to the morphology of MoS_2 [23], so the representative HRTEM micrographs of the different sulfided catalysts are shown in Fig. 2. Microscopically, supported MoS_2 is distributed asymmetrically in A1 and A2, but this microscopic asymmetry is difficult to track. Therefore, a macroscopically quantitative comparison of the lengths and layer numbers of MoS_2 slabs on the different catalysts was made through statistical analyses based on at least ten micrographs including 250–300 slabs taken from different parts of each catalyst.

The average slab lengths ($\bar{L}$) and stacking layer numbers ($\bar{N}$) were calculated according to the first moment of the distribution:

$$\bar{L}(\bar{N}) = \frac{\sum_{i=1}^{n} x_i M_i}{\sum_{i=1}^{n} x_i} \quad (5)$$

where M_i is the slab length or stacking layer number of a MoS_2 unit, and x_i the number of slabs or stacks in a given range of length or stacking layer number.

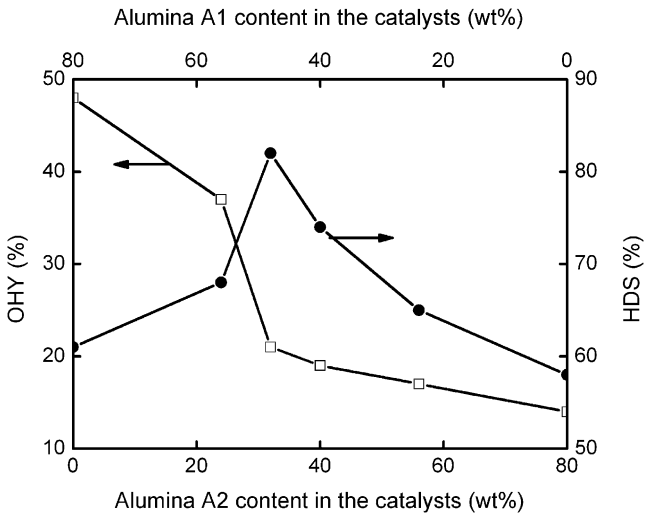

Fig. 4. Effects of catalyst composition on OHY and HDS activities over Catalysts CA1, CXA1-*YA2*, and CA2.

The relationships between the calculated average layer number and length of supported MoS_2 slabs and the catalyst composition in Table 3 show that the length and stacking layer number of MoS_2 slabs increase with the decreasing content of alumina A1 or the increasing content of alumina A2.

3.4. NO-IR

The IR spectra of adsorbed NO on the sulfided catalysts are shown in Fig. 3. The three bands at about 1860, 1785, and 1690 cm^{-1} are seen in the range of 2100–1500 cm^{-1}. The bands at about 1860 and 1785 cm^{-1} are assigned to NO adsorbed on the coordinatively unsaturated sites (CUS) of Mo sulfides and the bands at about 1785 and 1690 cm^{-1} are assigned to NO adsorbed on the CUS of Co sulfides [24]. The intensities of NO peaks derived from the Co and Mo sites decrease with the decreasing content of alumina A1 or the increasing content of alumina A2.

3.5. Catalytic performance

The effects of catalyst composition on the OHY and HDS activities are shown in Fig. 4. With the decreasing content of

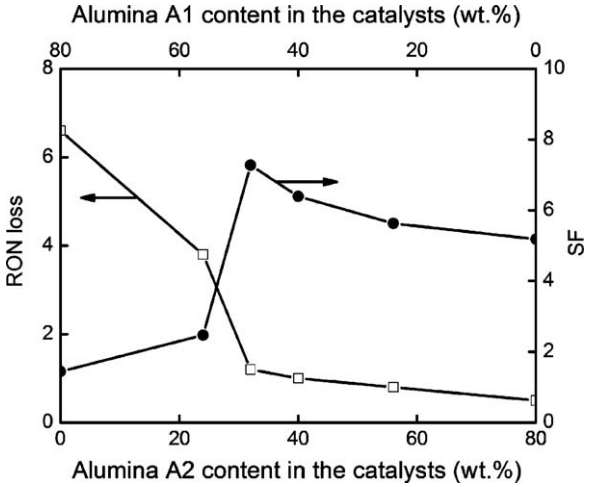

Fig. 5. Effects of catalyst composition on selectivity factor and RON loss over Catalysts CA1, CXA1-*YA2*, and CA2.

Table 4
Physicochemical properties and reaction performances of the catalysts supported on alumina A1.

Catalyst	Pore structure		Acidity		MoS_2 morphology		Activity	
	S_g [a] (m^2/g)	V_p [b] (mL/g)	A_a [c] (μmol NH_3/g_{cat})	A_s [d] (°C)	$\bar{L}$ [e] (nm)	$\bar{N}$ [e]	HDS (%)	OHY (%)
CA1	264	0.25	324	157	2.3	1.1	61	48
CA1-K1	263	0.25	269	156	2.3	1.1	59	37
CA1-K2	260	0.24	188	154	2.4	1.1	54	23

[a] BET surface area.
[b] Pore volume.
[c] Acid amount obtained by NH_3-TPD.
[d] Acid strength denoted by maximum NH_3 desorption temperature.
[e] Average slab length and stacking layer number obtained by the statistics analysis from different HRTEM micrographs.

Table 5
Physicochemical properties and reaction performances of the catalysts supported on silica.

Catalyst	Pore structure			Acidity		MoS_2 morphology		Activity	
	S_g [a] (m^2/g)	V_p [b] (mL/g)	D_p [c] (nm)	A_a [d] (μmol NH_3/g_{cat})	A_s [e] (°C)	$\bar{L}$ [f] (nm)	$\bar{N}$ [f]	HDS (%)	OHY (%)
CS1	568	0.59	4.2	124	143	2.9	1.0	50	21
CS2	532	0.65	4.9	112	141	3.0	1.0	49	21
CS3	473	0.76	6.4	94	139	2.9	1.0	48	19

[a] BET surface area.
[b] Pore volume.
[c] Mean pore diameter from $4 \times (V_p/S_g)$.
[d] Acid amount obtained by NH_3-TPD.
[e] Acid strength denoted by maximum NH_3 desorption temperature.
[f] Average slab length and stacking layer number obtained by the statistics analysis from different HRTEM micrographs.

alumina A1 or the increasing content of alumina A2, the OHY activity continuously decreases, while the HDS activity shows a maximum.

Decreasing the alumina A1 content or increasing the alumina A2 content reduces the product RON loss (Fig. 5), in coincidence with the dependence of the OHY activity on catalyst composition (Fig. 4). The selectivity factor shows a maximum with the change in catalyst composition, indicating that the optimum HDS selectivity can be achieved by adjusting the ratio of the two kinds of alumina in the catalysts.

From Figs. 4 and 5, we can conclude that the catalyst containing 48 wt.% A1 and 32 wt.% A2 has the highest HDS activity and selectivity among the six catalysts, giving a HDS ratio of 82%, an olefin saturation degree of about 20%, and a RON loss of 1.1 units.

4. Discussion

In order to elucidate the selective HDS performances of the above different catalysts, we will focus our discussion on the dependence of reaction performance on catalyst acidity and pore structure as well as on the structure of active metal sites by decoupling the effects of the three parameters.

4.1. Catalyst HDS and OHY activities versus acidity

To solely evaluate the effects of catalyst acidity on the HDS and OHY activities, Catalyst CA1 was modified by potassium to change its acidity and the physicochemical properties and reaction performances of the resulting catalysts are presented in Table 4. The incorporation of potassium of small quantity into CA1 can hardly influence the pore structure and MoS_2 morphology of the resulting catalyst, and this makes it possible to solely evaluate the effect of acidity on the catalyst HDS and OHY activities. From Table 4, one can see that the incorporation of alkali metal potassium greatly reduces the acid amount of CA1 with a slight effect on the acid strength of CA1, leading to the slightly decreased HDS activity and the remarkably weakened OHY activity, in accordance with the literature results [8,19,25]. However, the HDS activity in Table 3 shows a maximum with the decreasing acid amount in the acidity range of Table 4, which is remarkably different from the above-mentioned slightly decreased HDS activity with the decreasing acid amount in Table 4. Therefore, it can be concluded that the catalyst acidity cannot be the foremost factor influencing the catalyst HDS selectivity.

4.2. Catalyst HDS and OHY activities versus pore structure

The three silica-supported catalysts were prepared to solely evaluate the effect of pore structure on the HDS and OHY activities of catalysts and their physicochemical properties and reaction performances are presented in Table 5. Although the acidities of the three catalysts with different pore structures are different, the changes in their acid amounts are much less than those over the catalysts supported on alumina A1 (Table 4). Since the results in Section 4.1 have verified that the catalyst acidity is not the foremost factor influencing the catalyst HDS selectivity, the relatively minor changes in the acidities of the three silica-supported catalysts can be neglected. Xie et al. [26] demonstrated that the monolayer dispersion capacity of MoO_3 on silica gel is 0.028 g/100 m^2, so MoO_3 particles over the silica-supported catalysts are present in monolayer dispersion because the quantity of supported MoO_3 are lower than their monolayer dispersion capacity over the silica supports. Because the morphology of supported phases over oxidic catalysts matches with that over the resulting sulfided catalysts [27], the corresponding MoS_2 slabs should be monolayer. This inference is supported by the morphology of MoS_2 slabs with the average slab length of about 2.9 nm and the average stacking layer number of 1.0 over the three catalysts (Table 5). According to the above analysis, the pore structures of the three silica-supported catalysts can be solely correlated with their HDS and OHY activities in the case of the negligible difference of acidity and MoS_2 morphology. The correlation results in Table 5 show that the changes in the pore structures including surface area, pore volume, and pore diameter have a little effect on the HDS and OHY activities. As calculated by the quantum chemistry method [28], the kinetic diameters

(<0.7 nm) of the typical olefins and sulfur compounds in FCC gasoline are much smaller than the pore diameters (3.8–9.3 nm) of the catalysts, so no diffusion limitation effect exists for these reactants. Contrary to the above little effect of pore structure on the HDS and OHY activities, Table 3 shows that the OHY and HDS activities change greatly with the increasing pore diameter and the decreasing surface area of Catalysts CA1, CXA1-YA2, and CA2, so the catalyst pore structure should not be considered as the foremost factor influencing OHY and HDS reactions.

4.3. Catalyst HDS and OHY activities versus the structure of active metal sites

Since the catalyst acidity and pore structure are not the foremost factors influencing the selective HDS performance, the relationship between the selective HDS performance and the morphology of the main active component (MoS_2) was further pursued.

The MoS_2 dispersion, f_{Mo}, was calculated by dividing the total number of Mo atoms at the edge surface by the total number of Mo atoms. By assuming that MoS_2 slabs are present as perfect hexagons, the following equation was derived [29,30]:

$$f_{Mo} = \frac{\sum_{i=1,\ldots,t}(6n_i - 6)}{\sum_{i=1,\ldots,t}(3n_i^2 - 3n_i + 1)} \quad (6)$$

where n_i is the number of Mo atoms along one edge of a MoS_2 slab determined from its length ($L = 3.2(2n_i - 1)$ Å), and t is the total number of slabs shown in the TEM micrographs.

The stacking of supported MoS_2 slabs is defined as the average layer number.

The OHY activity, HDS activity, and selectivity factor over Catalysts CA1, CXA1-YA2, and CA2 were correlated with the dispersion and stacking of the supported MoS_2 slabs and the results are shown in Fig. 6. As seen in Fig. 6, the OHY activity increases with the increasing dispersion and decreasing stacking of the supported MoS_2 slabs, while the HDS activity displays a maximum at the dispersion of 0.33 and the stacking of 2.3 with the increasing MoS_2 dispersion and the decreasing MoS_2 stacking, similar to the trend of the selectivity factor.

The SCANfining technology for the selective HDS of FCC gasoline [31] has proved that the rim sites on MoS_2 slabs can catalyze both HDS and OHY reactions, but the edge sites can only catalyze the HDS reaction. Thus, a special catalyst with high HDS selectivity is developed via selectively poisoning the rim sites of MoS_2 slabs. Toba et al. [32] have verified that for the edge sites on the supported MoS_2 slabs the steric inhibition of the olefin molecules in FCC gasoline exists, consistent with the finding of the SCANfining techonology.

According to the above analysis, with the increasing dispersion and decreasing stacking of supported MoS_2 slabs, relatively more rim sites for olefin hydrogenation are formed and thereby the OHY activity is remarkably improved, as shown in Fig. 6a. This trend is in accordance with the favorable hydrogenation property of low-stacked MoS_2 slabs reported in literature [33,23].

The HDS activity shown in Fig. 6b can be explained as follows. When the dispersion is higher than 0.33 and the stacking is lower than 2.3, increasing dispersion and decreasing stacking lead to a rapid increase in the number of rim sites with the steric hindrance, which is unfavorable for the HDS of benzothiophenes that takes a share of about 25% in the total sulfur of FCC gasoline [34], so the catalyst HDS activity is weakened due to the restrained adsorption of benzothiophenes (Fig. 7a). When the dispersion is lower than 0.33 and the stacking is higher than 2.3, increasing stacking and decreasing dispersion of the supported MoS_2 slabs lead to a poor dispersion of edge sites favorable for the HDS reaction [35] and thus part of thiophenes and benzothiophenes diffuse into the gas phase during their movement to the edge sites, so the catalyst HDS activity is greatly reduced (Fig. 7c).

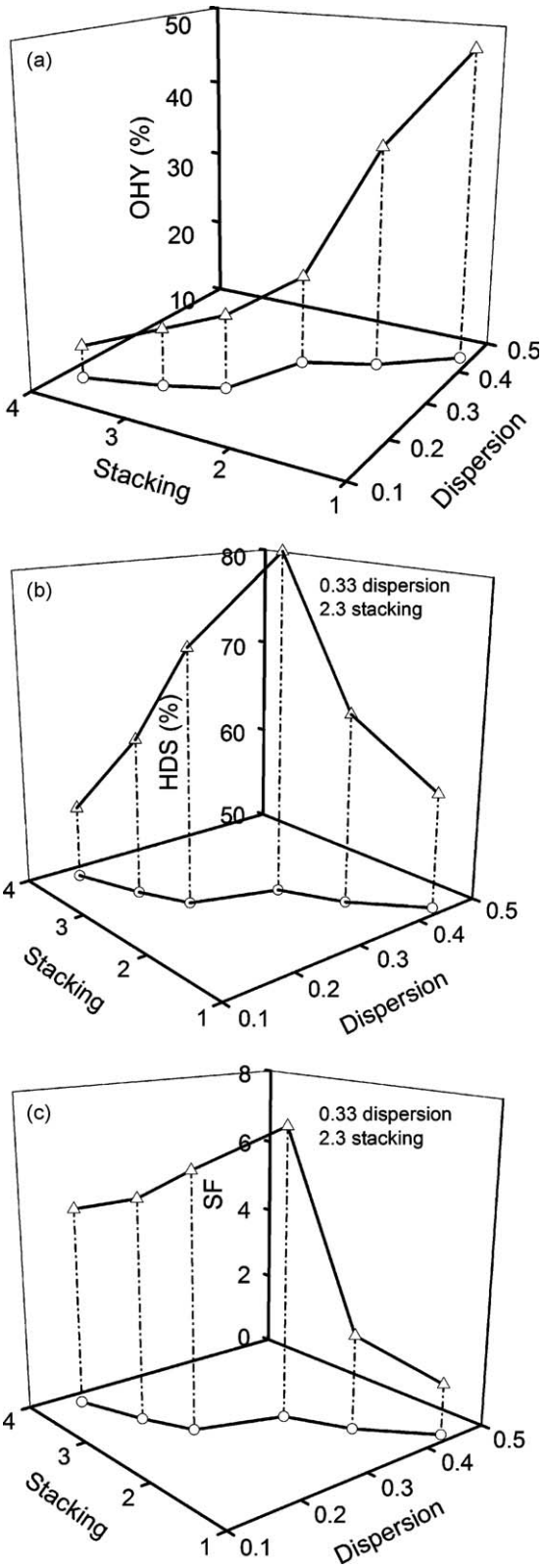

Fig. 6. OHY activity (a), HDS activity (b) and selectivity factor (c) versus the dispersion and stacking of supported MoS_2 slabs over Catalysts CA1, CXA1-YA2, and CA2.

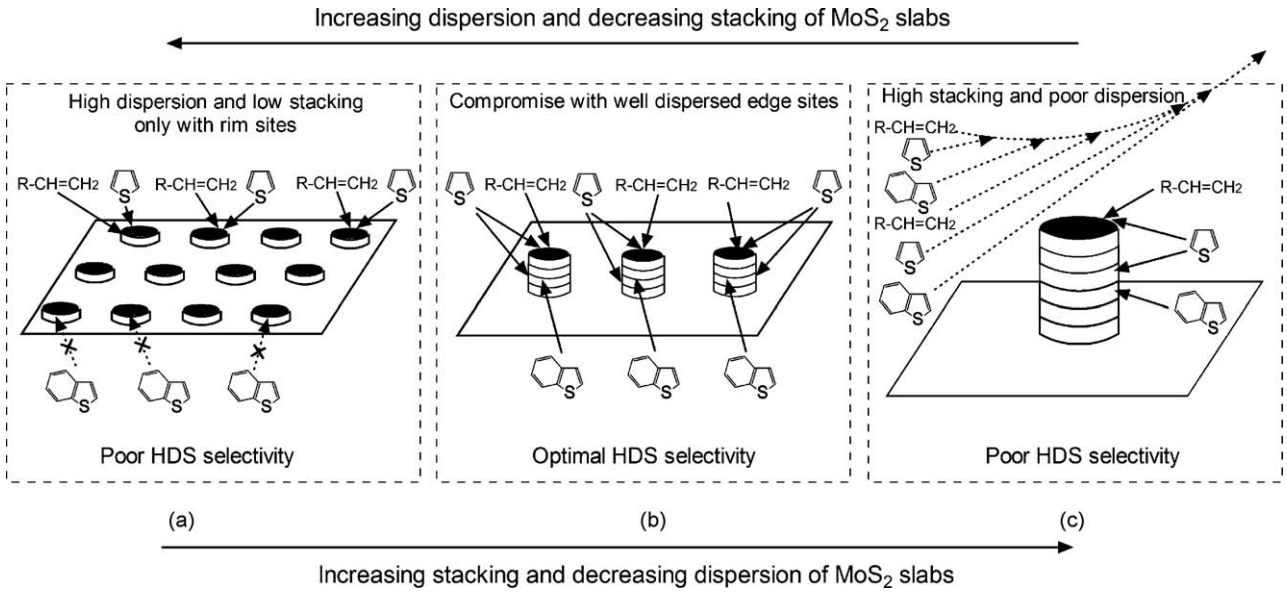

Fig. 7. Schematic representation for optimizing the dispersion and the stacking of supported MoS_2 slabs for the selective HDS of FCC gasoline.

For the catalyst with a dispersion of 0.33 and a stacking of 2.3, a compromise between the dispersion and the stacking of supported MoS_2 slabs is accomplished. This catalyst has sufficient and accessible edge sites and suitable rim sites (Fig. 7b) and thus has an optimal HDS selectivity, as shown in Fig. 6c.

Noticeably, the results in Fig. 6b show that at the high dispersion of 0.44 and the low stacking of 1.1 a desulfurization ratio of 61% was achieved in spite of the adsorption of olefins on only rim sites, indicating the effective occurrence of the HDS reaction despite the predominance of rim sites on the catalyst surface. In view of the steric hindrance of rim sites for benzothiophenes in FCC gasoline, the removed sulfur species should be mainly assigned to about 50% thiophenes in the total sulfur of FCC gasoline [36]. Removal of thiophenes on the rim sites of supported MoS_2 slabs can be well explained by the Brim theory [37–39]. According to this theory that was demonstrated by density functional theory and various microscopy characterizations, Besenbacher et al. [37] and Topsøe et al. [38,39] proposed that the rim sites of MoS_2 slabs are able to hydrogenate thiophene to 2,5-dihydrothiophene, and these sites are also able to break the S–C bond of thiophene to produce cis-2-butenethiolate. The proposal indicates that the rim sites of MoS_2 slabs have two functions of hydrogenation and hydrogenolysis. Therefore, thiophenic sulfides in FCC gasoline can be removed by initial hydrogenation and subsequent S–C scission on the rim sites.

The above discussion on thiophene HDS on the rim sites of supported MoS_2 slabs supports the deduction that both rim and edge sites are active for thiophene HDS.

To further demonstrate the reaction properties of rim and edge sites over supported MoS_2 slabs, the ratios (R) of edge sites to rim sites were calculated as follows:

$$R = \frac{\sum_{j=3}^{7} x_j j - 2\sum_{j=3}^{7} x_j}{k + 2(t-k)} \quad (7)$$

where j is the stacking layer number of a MoS_2 unit, x_j is the number of j layer stacks, k is the number of mono-layer MoS_2 slabs, and t is the total number of slabs shown in the TEM micrographs.

The ratios of edge sites to rim sites were correlated with the OHY and HDS activities and the results are shown in Fig. 8. With the increasing edge/rim ratio, the OHY decreases, whereas the HDS activity firstly increases and then decreases. These results confirm the selectivity of the rim sites for the OHY reaction, but they are not consistent with the selectivity of the edge sites for the HDS reaction in the case of the edge/rim ratio >0.6. With the higher edge/rim ratio, more edge sites are formed at the cost of their deteriorated dispersion on supports [40], so the adsorption of sulfur species on the edge sites is restrained and thus the HDS activity is weakened.

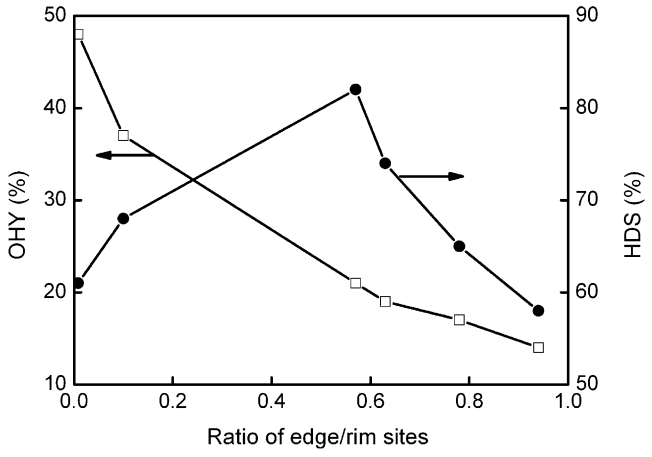

Fig. 8. OHY and HDS activities versus the ratios of edge sites to rim sites of MoS_2 slabs over Catalysts CA1, CXA1-YA2, and CA2.

To elucidate the effects of the structure of active metal sites on the reaction performances of catalysts, the OHY activity, HDS activity, and selectivity factor over Catalysts CA1, CXA1-YA2, and CA2 were correlated with the absorbances of the IR bands of adsorbed NO on the CUSs of Co and Mo sulfides and the results are shown in Fig. 9. The OHY activity increases with the increasing Co and Mo CUSs reflected by their peak heights, whereas the HDS activity shows a maximum with the increasing Co and Mo CUSs, similar to the trend of the selectivity factor.

Combining Figs. 9a and 10, one can see that with the increasing dispersion or decreasing stacking of supported MoS_2 slabs, the Co and Mo CUSs increase, possibly because of the weakened interaction between Co and Mo atoms for MoS_2 slabs with high

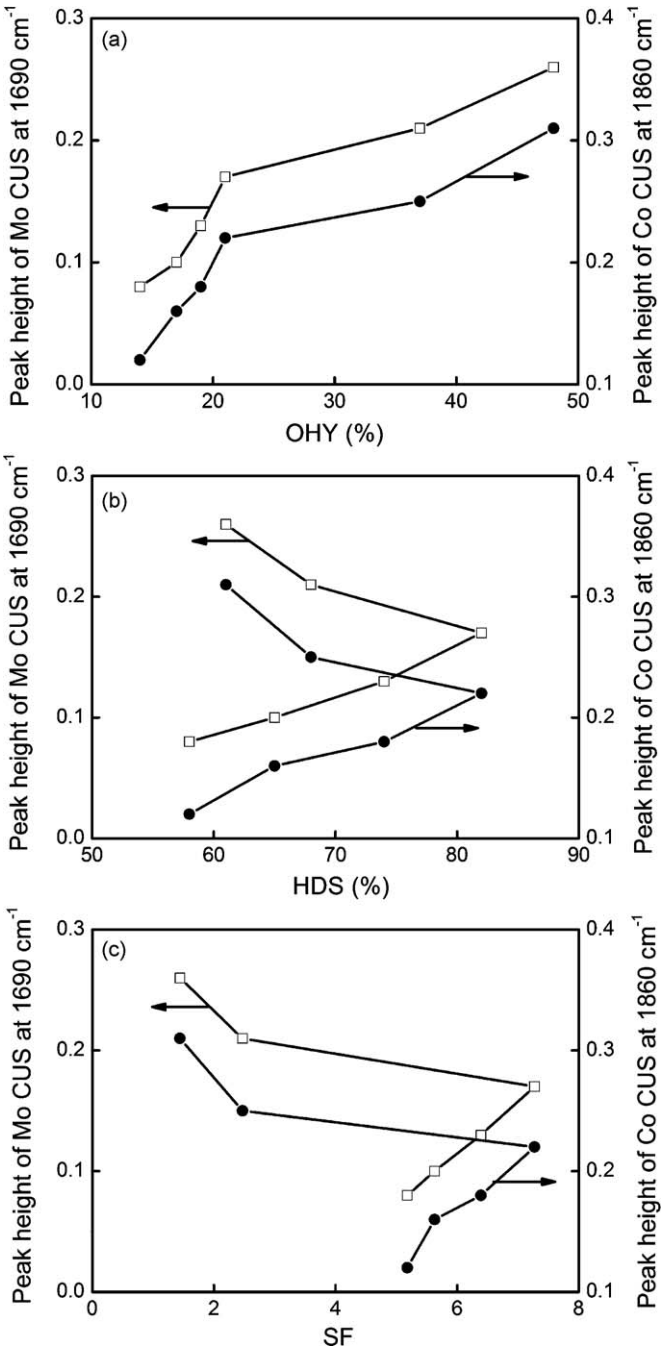

Fig. 9. Absorbances of the IR bands of adsorbed NO on the CUSs of Co and Mo sulfides (peak heights at 1860 and 1690 cm^{-1}, respectively) versus OHY activity (a), HDS activity (b), and selectivity factor (c) over Catalysts CA1, CXA1-YA2, and CA2.

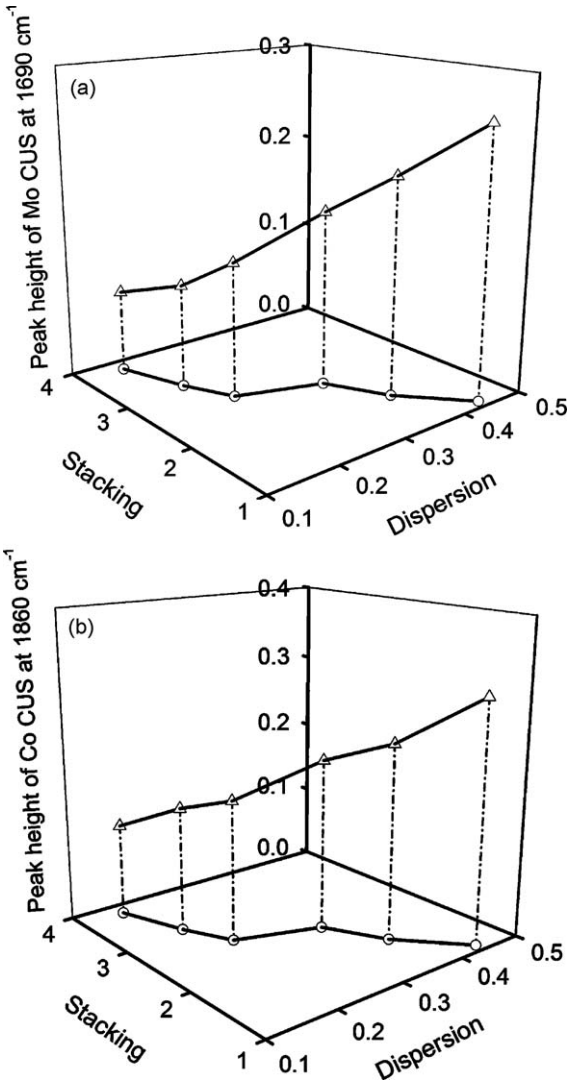

Fig. 10. Absorbances of the IR bands of adsorbed NO on the CUSs of Mo (a) and Co (b) sulfides (peak heights at 1690 and 1860 cm^{-1}, respectively) versus the dispersion and stacking of supported MoS_2 slabs over Catalysts CA1, CXA1-YA2, and CA2.

dispersion and low stacking. Thus, the more exposed rim sites of MoS_2 slabs for olefin saturation result in the increase of the OHY activity.

From Figs. 9b and 10, the high dispersion and low stacking of MoS_2 slabs increase the number of Co and Mo CUSs and thus reduce the active Co–Mo–S phases [41], so the corresponding HDS activity is undesirable. On the other hand, although the high stacking and low dispersion of MoS_2 slabs can promote the formation of Co–Mo–S phases, as evidenced by the low peak heights of Co and Mo CUSs [42], the poor accessibility of the active phases for sulfur species as discussed above leads to the low HDS activity. Therefore, the compromise between the dispersion and the stacking of MoS_2 slabs is necessary to form the sufficient and accessible Co–Mo–S phases for achieving optimal HDS selectivity.

5. Conclusions

The physicochemical properties of Co–Mo–Mg/Al_2O_3, K–Co–Mo–Mg/Al_2O_3, and Co–Mo/silica catalysts were correlated with their hydrodesulfurization (HDS) and olefin hydrogenation activities. The results showed that compared with the pore structure and acidity of the catalysts, the MoS_2 morphology could better explain the HDS selectivity. High dispersion and low stacking of supported MoS_2 slabs increased the number of active adsorption sites for olefins and thus promoted the catalyst olefin hydrogenation activity, leading to an undesirable HDS selectivity. High stacking and low dispersion of supported MoS_2 slabs decreased the number of olefin adsorption sites, but the poor accessibility of the sulfur adsorption sites gave the corresponding catalyst unsatisfactory HDS activity and selectivity. For an ideal catalyst that can selectively hydrodesulfurize FCC gasoline, a compromise between the dispersion and the stacking of supported MoS_2 slabs is crucial. The findings obtained in the present investigation shed a light for the rational design of supported MoS_2 catalysts.

Acknowledgements

This work was supported by the National Basic Research Program of China (Grant No. 2004CB217807), the Natural Science Foundation of China (Grant No. 20606037 and Grant No. 20825621), and the New Star Plan of Beijing (Grant No. 2007B073).

References

[1] S. Brunet, D. Mey, G. Pérot, C. Bouchy, F. Diehl, Appl. Catal. A: Gen. 278 (2005) 143–172.
[2] F. Trejo, M.S. Rana, J. Ancheyta, Catal. Today 130 (2008) 327–336.
[3] M. Toba, Y. Miki, Y. Kanda, T. Matsui, M. Harada, Y. Yoshimura, Catal. Today 104 (2005) 64–69.
[4] D. Solis, T. Klimova, J. Ramírez, T. Cortez, Catal. Today 98 (2004) 99–108.
[5] O. Sadakane, Y. Sasaki, R. Ohnishi, EP Patent 0,745,660 (2000).
[6] S. Hatanaka, M. Yamada, O. Sadakane, Ind. Eng. Chem. Res. 37 (1998) 1748–1754.
[7] S. Hatanaka, O. Sadakane, S. Hikita, T. Miyama, US Patent 5,853,570 (1998).
[8] Y. Fan, J. Lu, G. Shi, H. Liu, X. Bao, Catal. Today 125 (2007) 220–228.
[9] S. Srinivasan, A.K. Datye, C.H.F. Peden, J. Catal. 137 (1992) 513–522.
[10] A.K. Datye, S. Srinivasan, L.F. Allard, C.H.F. Peden, J.R. Brenner, L.T. Thompson, J. Catal. 158 (1996) 205–216.
[11] T. Klicpera, M. Zdražil, J. Catal. 206 (2002) 314–320.
[12] J. Cinibulk, P.J. Kooyman, Z. Vit, M. Zdražil, Catal. Lett. 89 (2003) 147–152.
[13] J.T. Miller, W.J. Reagan, J.A. Kaduk, C.L. Marshall, A.J. Kropf, J. Catal. 193 (2000) 123–131.
[14] K. Inamura, R. Prins, Stud. Surf. Sci. Catal. 92 (1995) 401–412.
[15] J.-S. Choi, C. Petit-Clair, D. Uzio, Stud. Surf. Sci. Catal. 143 (2002) 585–592.
[16] S. Hatanaka, M. Yamada, O. Sadakane, Ind. Eng. Chem. Res. 36 (1997) 5110–5117.
[17] J.-S. Choi, F. Maugé, C. Pichon, J. Oliver-Fourcaded, J.C. Jumas, C. Petit-Clair, D. Uzio, Appl. Catal. A: Gen. 267 (2004) 203–216.
[18] R. Candia, O. Sørensen, J. Villadsen, N.-Y. Topsøe, B.S. Clausen, H. Topsøe, Bull. Soc. Chim. Belg. 93 (1984) 763–773.
[19] D. Mey, S. Brunet, C. Canaff, F. Maugé, C. Bouchy, F. Diehl, J. Catal. 227 (2004) 436–447.
[20] S.G. Kukes, P.D. Hopkins, L.A. Ollendorff, P.D. Hendler, C.D. Ontiveros, D.M. Washecheck, US Patent 5,348,928 (1994).
[21] C. Bai, G.B. McVicker, S.S. Shih, M.C. Kerby, E.A. Lemon JR., US Patent 0,049,083A1 (2006).
[22] F. Arena, R. Dario, A. Parmaliana, Appl. Catal. A: Gen. 170 (1998) 127–137.
[23] H. Shimada, Catal. Today 86 (2003) 17–29.
[24] T. Mochizuki, H. Itou, M. Toba, Y. Miki, Y. Yoshimura, Energ. Fuel 22 (2008) 1456–1462.
[25] T. Klimova, D.S. Casados, J. Ramírez, Catal. Today 43 (1998) 135–146.
[26] Y. Xie, Y. Tang, Adv. Catal. 37 (1990) 1–43.
[27] S. Dzwigaj, C. Louis, M. Breysse, M. Cattenot, V. Bellière, C. Geantet, M. Vrinat, P. Blanchard, E. Payen, S. Inoue, H. Kudo, Y. Yoshimura, Appl. Catal. B: Environ. 41 (2003) 181–191.
[28] Y. Pan, D. Wang, J. Gao, Acta Petrol. Sin. 23 (2007) 63–67.
[29] E.J.M. Hensen, P.J. Kooyman, Y. van der Meer, A.M. van der Kraan, V.H.J. de Beer, J.A.R. van Veen, R.A. van Santen, J. Catal. 199 (2001) 224–235.
[30] S. Kasztelan, H. Toulhoat, J. Grimblot, J.P. Bonnelle, Appl. Catal. 13 (1984) 127–159.
[31] T.G. Kaufmann, A. Kaldor, G.F. Stuntz, M.C. Kerby, L.L. Ansell, Catal. Today 62 (2000) 77–90.
[32] M. Toba, Y. Miki, T. Matsui, M. Harada, Y. Yoshimura, Appl. Catal. B: Environ. 70 (2007) 542–547.
[33] Y. Sakashita, Y. Araki, H. Shimada, Appl. Catal. A: Gen. 215 (2001) 101–110.
[34] T.A. Zepeda, B. Pawelec, J.L.G. Fierro, T. Halachev, Appl. Catal. B: Environ. 71 (2007) 223–236.
[35] H. Farag, Appl. Catal. B: Environ. 84 (2008) 1–8.
[36] Y. Miki, M. Toba, Y. Yoshimura, J. Jpn. Petrol. Inst. 51 (2008) 225–233.
[37] F. Besenbacher, M. Brorson, B.S. Clausen, S. Helveg, B. Hinnemann, J. Kibsgaard, J.V. Lauritsen, P.G. Moses, J.K. Nørskov, H. Topsøe, Catal. Today 130 (2008) 86–96.
[38] H. Topsøe, B. Hinnemann, J.K. Nørskov, J.V. Lauritsen, F. Besenbacher, P.L. Hansen, G. Hytoft, R.G. Egeberg, K.G. Knudsen, Catal. Today 107–108 (2005) 12–22.
[39] H. Topsøe, Appl. Catal. A: Gen. 322 (2007) 3–8.
[40] Z. Yu, L.E. Fareid, K. Moljord, E.A. Blekkan, J.C. Walmsley, D. Chen, Appl. Catal. B: Environ. 84 (2008) 482–489.
[41] R. Nava, R.A. Ortega, G. Alonso, C. Ornelas, B. Pawelec, J.L.G. Fierro, Catal. Today 127 (2007) 70–84.
[42] N.-Y. Topsøe, H. Topsøe, J. Catal. 84 (1983) 386–401.